Journal of Civil Structural Health Monitoring (2025) 15:2229–2243
https://doi.org/10.1007/s13349-025-00931-z

ORIGINAL PAPER

Operational modal damping identification based on compressive sensing

Jian Zhou[1,2] · Hong-Wei Li[2] · You-Wu Wang[2] · Yi-Qing Ni[2]

Received: 18 March 2024 / Accepted: 17 February 2025 / Published online: 5 March 2025

Abstract
Modal damping is a crucial parameter for structural condition and damage assessment. The modal identification using incomplete measurements can be realized by techniques based on Compressive Sensing (CS), which can reduce the amount of data for transmission and improve computational efficiency. However, techniques, such as sparse decomposition with prior information (SDPI), may hardly realize modal damping identification with satisfied precision under ambient vibration. To improve both the efficiency and precision, a novel CS-based modal damping identification method is presented, called Damping Identification by Sparse Decomposition (DISD). A random compression sampling scheme, random sampling with subsamples, is proposed to realize DISD. To enhance the damping identification accuracy, a new formula is proposed. Studies on numerical examples and real monitoring data from the Tsing Ma bridge were conducted for verification. The effectiveness of the presented DISD method is compared with that of the CS-based and traditional methods. Both the numerical and the real-monitoring cases show that DISD has improved modal damping results. Therefore, the proposed method is an efficient operational modal analysis tool and has the potential to be adopted in civil engineering practice.

Keywords Structural health monitoring · Modal damping identification · Compressed measurements · Compressive sensing

1 Introduction

Infrastructures include bridges [1, 2], dams [3], and buildings [4], need continuous structural health monitoring (SHM) to evaluate their structural conditions [5, 6]. Modal parameters, e.g., modal frequency, modal damping, and mode shape, are fundamental dynamic characteristics for vibration-based SHM systems. Operational Modal Analysis (OMA) is able to estimate modal parameters only from the responses of structures. Unlike the traditional experimental modal analysis, OMA does not require measurements of excitations. Therefore, it has been widely used for SHM systems [7–9].

A critical problem for continuous SHM is that a vast amount of data is generated, which leads to challenges for data transmission, storage, and analysis. Since enormous data may cause degraded battery life and frequent maintenance of sensors, the problem is becoming increasingly serious for wireless sensor networks [10, 11]. On the premise of ensuring the accuracy of parameter identification, sampling less data is necessary for long-term SHM. While conventional techniques, such as automated frequency domain decomposition (AFDD) [12], need to comply with the sampling rate (more than two times the highest identified frequency) for sampling measurements. Therefore, these methods can hardly be applied to compressed measurements. To overcome this restriction, the powerful mathematical theory compressive sensing (CS) was proposed to collect measurements at a sub-Nyquist sampling rate [13, 14]. Since CS can construct useful information from compressed measurements, it can resolve the problem of collecting data with minimal power consumption [13]. As a result, numerous CS-based monitoring techniques have been established for long-term SHM systems [15–17].

✉ Hong-Wei Li
hong-wei.li@polyu.edu.hk

[1] Department of Architecture and Civil Engineering, City University of Hong Kong, Kowloon, Hung Hom, Kowloon, Hong Kong

[2] Department of Civil and Environmental Engineering, National Rail Transit Electrification and Automation Engineering Technology Research Center (Hong Kong Branch), The Hong Kong Polytechnic University, Hong Kong, China

CS-based modal parameter identification typically requires the reconstruction of original measurements [18–21], which results in information leakage and additional computational burdens. In attempting to mitigate these problems, Park et al. [22] first presented the proper orthogonal decomposition technique to identify mode shapes via incomplete measurements. They demonstrated that this method can also be applied to damped cases [23]. Kang and Duan [24] introduced the sparse decomposition method by searching for a dictionary to identify all modal parameters. The results showed that the proposed method performs well with compressed measurements of damped systems under free vibration. To realize CS-based OMA, Zhou et al. [25] presented the sparse decomposition with prior information (SDPI) to identify natural frequencies and mode shapes from compressed measurements of damped cases under ambient vibration. The method uses the last identified modal parameter results as prior information to make current modal identification more accurate. The initial prior information is acquired from a traditional OMA method which is applied to uncompressed measurements. Despite the existing CS-based modal identification methods have been thoroughly verified in terms of the accuracy and efficiency for the modal frequency and mode shape identification, they cannot be used to identify modal damping from compressed measurements under ambient vibration. The lack of modal damping identification leads to a lower quality OMA.

Modal damping is a fundamental parameter for OMA and one of the most important indices for SHM. It can be used for condition monitoring [26], damage identification [27], and vibration control [28]. Therefore, modal damping identification has been investigated extensively [29, 30]. Prior to determining modal damping, the free vibration responses need to be derived from the responses under ambient vibration by signal processing techniques. James et al. [31] introduced the natural excitation technique (NExT) to derive free vibration responses by calculating the cross-correlation function. The traditional modal analysis methods can be applied to identify modal damping under ambient vibration after applying NExT. Differing from the traditional modal analysis methods, the CS-based methods are executed with compressed measurements. For NExT, the time intervals between adjacent sampled time points must be consistent, while that of the compressed measurements collected by the existing random sampling scheme are normally not. Specifically, the traditional random sampling scheme, namely the non-uniform low-rate random sampling scheme, is to pick L random samples for sampling measurements. Since the requirement of NExT cannot be satisfied straightforwardly, the CS-based methods can hardly identify modal damping from random vibration responses. Therefore, designing a new random compression sampling scheme to realize CS-based modal damping identification is worthwhile.

This study presents a method called Damping Identification by Sparse Decomposition (DISD) to identify modal damping using the CS technique from random responses. The innovations/contributions of this paper are: (i) A new random compression sampling scheme, random sampling with subsamples, is designed to meet the requirement of NExT, thus CS-based modal damping identification under ambient vibration is realized; (ii) A new formula is proposed for a CS-based algorithm to improve the accuracy. Both the response data from a numerical damped system and the monitoring data from Tsing Ma bridge under ambient vibration are adopted to verify the accuracy of DISD. The proposed DISD is compared to the CS-based OMA method SDPI and the traditional methods AFDD and COVariance-driven Stochastic Subspace Identification (SSI-COV) [32].

2 Methodology

In this section, we first briefly introduce AFDD and SSI-COV. Second, we propose a random sampling scheme for the execution of NExT. Third, we decompose the signals of the linear system under ambient vibration to explain the theory of CS-based modal damping identification. Next, we propose a new identification formula to enhance the accuracy of identified modal damping results. Finally, we introduce the process of modal damping identification based on the sparse representation produced by the CS algorithm.

2.1 The introduction of AFDD and SSI-COV

AFDD is a widely adopted frequency domain modal analysis method, it identifies modal parameters using power spectral density. First, responses are used to calculate power spectral density. Next, singular value decomposition is applied to calculate singular values and singular vectors of the power spectral density. Finally, the modal parameters are extracted by the singular values and singular vectors.

As a powerful time domain modal analysis method, SSI-COV uses state space model to realize modal identification. The covariance matrix is calculated using responses. Then, the covariance matrix is used to compose block Toeplitz matrix. The singular values and singular vectors are calculated using singular value decomposition from the block Toeplitz matrix. Finally, the modal parameters are identified from the singular values and singular vectors.

2.2 Random sampling with subsamples

The existing sampling schemes can hardly be directly utilized for modal damping identification under ambient excitation. In this study, we propose a new random compression

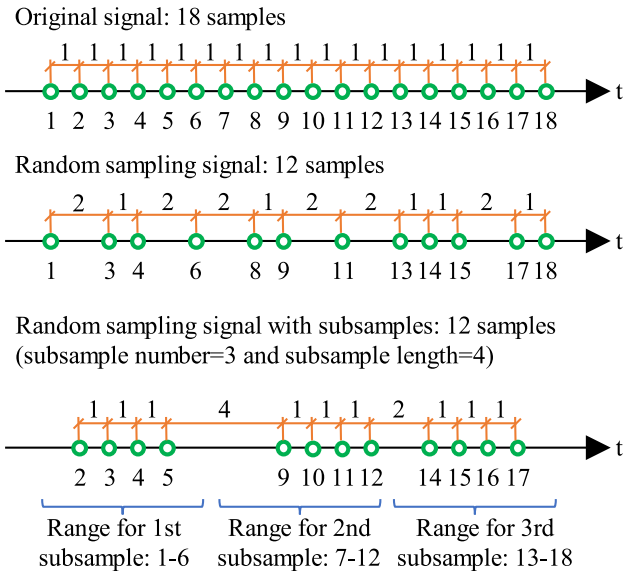

Fig. 1 Schematic diagram of the random sampling scheme and random sampling with subsamples scheme

sampling scheme to address this problem, namely random sampling with subsamples.

The principle of the proposed scheme is to replace single samples with subsamples. The length of subsamples can be set by users. The number of subsamples is the compressed signal length divided by the length of subsamples. The interval between samples within each subsample is fixed. However, the time interval between adjacent subsamples is still random. To avoid excessive time intervals between subsamples, we divide same-sized ranges for each subsample. The size of each range is equal to the original sample length divided by the number of subsamples. Figure 1 shows the illustration of the proposed random sampling with subsamples compression sampling scheme.

From Fig. 1, we can find that the sample length of the original signal is 18 and the time interval between adjacent sampled time points is consistent. For both the two random compression sampling schemes, the compression ratio of the compressed signal is 66.7% and the sample length is 12. In this illustrated example, the sample length of each subsample is set to 4, and the number of subsamples is 3. Each subsample collected by the proposed scheme can satisfy the requirement for the calculation of the cross-correlation function, which makes NExT workable. We can use NExT to derive the free vibration responses from the ambient vibration responses. Since the existing CS-based methods can identify modal damping from free vibration responses, we can identify modal damping results from each subsample. For all subsamples of the compressed signal, the results of modal damping are determined individually. The overall modal damping is obtained by taking the average of the results from all subsamples. By following the abovementioned procedure, the modal damping can be extracted from compressed random responses. The advantage of the proposed scheme is that it is effective and easy to implement.

2.3 Signal decomposition

The vibration equation of a simple system with N degree of freedom under ambient excitation is:

$$\mathbf{M}\ddot{x}(t) + \mathbf{C}\dot{x}(t) + \mathbf{K}x(t) = \mathbf{F}(t) \tag{1}$$

where $\mathbf{M}$, $\mathbf{C}$, and $\mathbf{K}$ are the $N \times N$ matrices of mass, damping, and stiffness, respectively; $x(t)$ is the vector of displacement, respectively; $\mathbf{F}(t)$ is the excitation vector.

The incomplete measurements $\mathbf{Y}$ with discretized time t ($t_1, \ldots, t_M$, $M \gg N$) can be expressed as:

$$\mathbf{Y}_{N\times L} = \mathbf{X}_{N\times M}\mathbf{\Phi}_{M\times L} \tag{2}$$

where $\mathbf{X}$ is the original uncompressed measurement matrix; $\mathbf{\Phi}$ is a random matrix which is used for compressing $\mathbf{X}$. L is the compressed measurement length ($M \gg L$). Since the compressed measurements are collected by the proposed compression sampling scheme, they can be divided into subsamples.

The signal processing technique NExT is utilized to derive the free vibration responses from the ambient vibration responses for all subsamples one by one. According to James et al. [31], NExT assumes that the measurements are collected from time-invariant linear systems and the excitation is independent of the collected measurements. The fundamental theory of NExT is to calculate the cross-correlation function of responses of the ambient vibration responses. Since the cross-correlation function $\mathbf{R}$ can be regarded as the free vibration responses of the identified system [31], $\mathbf{R}$ of each subsample can be expressed as:

$$\mathbf{R}(T) = \sum_{j=1}^{N} \boldsymbol{\psi}_j A_j \exp\left(-\xi_j \omega_{n,j} T\right) \sin\left(\omega_{d,j} T + \theta_j\right) \tag{3}$$

where $\boldsymbol{\psi}_j$ is the j^{th} mode shape vector; A_j is the coefficient of the jth mode; $\omega_{n,j}$ and $\omega_{d,j}$ are the j^{th} undamped and damped modal frequency, respectively; ξ_j is the jth modal damping ratio; T ($T = 0, \Delta t, 2\Delta t, \ldots, T_{\text{Max}}$, T_{Max} is the maximum time separation) is the time separation, and the length of T is

$Q = \left(\frac{T_{\text{Max}}}{\Delta t}\right) + 1$; θ_j is the phase of the jth mode. The parameters of NExT, such as T and reference channel ($\mathbf{R}$ is calculated between the reference channel and all channels) need to be set by users. Detailed discussions about these settings can be found in [31]. Note that the number of rows in $\mathbf{R}$ is P, which is equal to the number of reference channels multiplied by N. The length of $\mathbf{R}$ is equal to the length of T. Following [24, 25], $\mathbf{R}$ is determined by the time separation T for each reference channel and it can also be expressed as:

$$\mathbf{R}_{N\times Q} = \mathbf{\Psi}_{N\times N}\mathbf{\Gamma}_{N\times 2N}\mathbf{S}_{2N\times Q} \tag{4}$$

where $\mathbf{\Psi}$ is the mode shape matrix; $\mathbf{\Gamma} = \left[\mathbf{\Gamma}'\mathbf{\Gamma}''\right]$ is the coefficient matrix, $\mathbf{\Gamma}'$ and $\mathbf{\Gamma}''$ are $N \times N$ diagonal matrices with elements $A_j{}' = A_j \cos\left(\theta_j\right)$ and $A_j'' = A_j \sin\left(\theta_j\right)$, respectively; $\mathbf{S} = \left[\mathbf{S}'\mathbf{S}''\right]^{\mathrm{T}}$ is the modal coordinate matrix, $\mathbf{S}'$ and $\mathbf{S}''$ are $N \times Q$ matrices with elements: $s_j{}'(T) = \exp\left(-\xi_j\omega_{n,j}T\right)\sin\left(\omega_{d,j}T\right)$ and $s_j''(T) = \exp\left(-\xi_j\omega_{n,j}T\right)\cos\left(\omega_{d,j}T\right)$.

According to [24, 25], the dictionary $\mathbf{D}$ is designed to include $\mathbf{S}$, and the coefficient $\mathbf{\Upsilon}$ is designed to include $\mathbf{\Psi\Gamma}$. Therefore, $\mathbf{R}$ can be re-expressed as:

$$\mathbf{R} = \mathbf{\Upsilon D} \tag{5}$$

Since $\mathbf{R}$ follows the CS formula of Eq. (5), CS-based techniques are able to identify modal damping.

2.4 Damping dictionary design

After processing signals by NExT, the damping dictionary $\mathbf{D}$ is formed to identify modal damping for the cross-correlation function of each subsample. General bases of $\mathbf{D}$ include the free vibration function, the discrete sine transform, the discrete cosine transform, and the Hilbert transform. In this study, $\mathbf{D}$ is created based on the free vibration function. The same base in SDPI is used for DISD for comparison. It should be noted that alternative bases can also be employed for CS-based modal damping identification. According to [24, 25], $\mathbf{D}$ contains each modal damping ratio ξ_m ($m \in 1, \ldots, q$) from the possible minimum value to the maximum one $\left[\xi_{min}, \xi_{max}\right]$. Since the length of $\mathbf{D}$ is equal to the length of T, $\mathbf{D}$ is a $2q \times Q$ matrix for each subsample. $\mathbf{D}$ can be expressed as:

$$\mathbf{D} = \left[\mathbf{D}'\mathbf{D}''\right]^{\mathrm{T}} = \begin{bmatrix} d_{1,1}{}' & \cdots & d_{1,Q}{}' \\ \vdots & \ddots & \vdots \\ d_{q,1}{}' & \cdots & d_{q,Q}{}' \\ d_{1,1}'' & \cdots & d_{1,Q}'' \\ \vdots & \ddots & \vdots \\ d_{q,1}'' & \cdots & d_{q,Q}'' \end{bmatrix} \tag{6}$$

One atom represents a possible modal damping ratio. Each atom in $\mathbf{D}$ includes two parts: d' (the atom of $\mathbf{D}'$) and d'' (the atom of $\mathbf{D}''$). The element of atoms d' and d'' can be expressed as:

$$\begin{aligned} d' &= \exp\left(-\frac{\xi_m\omega_d T}{\sqrt{1-\xi_m^2}}\right)\sin\left(\omega_d T\right) \text{ and} \\ d'' &= \exp\left(-\frac{\xi_m\omega_d T}{\sqrt{1-\xi_m^2}}\right)\cos\left(\omega_d T\right) \end{aligned} \tag{7}$$

2.5 Modal damping identification

When the dictionary is created, sparse representation can be carried out by the powerful CS algorithm orthogonal matching pursuit (OMP) [33]. In this study, the same CS algorithm for SDPI is used for DISD. However, other CS algorithms can also be used for CS-based modal damping identification. Then, OMP is used to solve the optimization function of modal damping identification under ambient vibration. Figure 2 visualizes the flowchart of DISD from sampling compressed measurements to modal damping identification.

The number of atoms of $\mathbf{D}$ needs to be redundant ($q \gg N$). Ideally, the coefficient matrix $\mathbf{\Upsilon}$ contains N elements with large values and many elements with small values. Therefore, the cross-correlation function $\mathbf{R}$ is sparse. In this study, the OMP algorithm is adopted to find the optimal solutions ($\hat{\mathbf{D}}$ and $\hat{\mathbf{\Upsilon}}$). The optimization function is:

$$\min \left\|\mathbf{R} - \hat{\mathbf{\Upsilon}}\hat{\mathbf{D}}\mathbf{\Phi}\right\|_2 \text{ s.t.} \hat{\mathbf{D}} \in \mathbf{D} \tag{8}$$

where $\hat{\mathbf{D}}$ contains N optimal atoms extracted from $\mathbf{D}$ and $\hat{\mathbf{\Upsilon}}$ (with large value elements) is the coefficient matrix of $\hat{\mathbf{D}}$. Larger value for elements of $\hat{\mathbf{\Upsilon}}$ means that the corresponding atom contributes more to $\mathbf{R}$. Therefore, we can identify modal damping from $\hat{\mathbf{D}}$ since $\hat{\mathbf{D}}$ is the optimal approximation of $\mathbf{S}$.

The identification order of the existing CS techniques, e.g., SDPI, is modal frequency to modal damping to mode shape. The modal frequencies are considered as the basic information used to identify modal damping results. The CS-based OMA techniques can accurately identify both modal frequency and mode shape using compressed measurements. Since the identification of modal damping is more easily affected than that of modal frequency and mode shape, we consider a new identification order, namely modal frequency to mode shape to modal damping. In the proposed order, the identification of modal frequency and mode shape is conducted before identifying modal damping. Both the identified modal frequencies and mode shapes by the existing CS techniques, such as SDPI, are considered

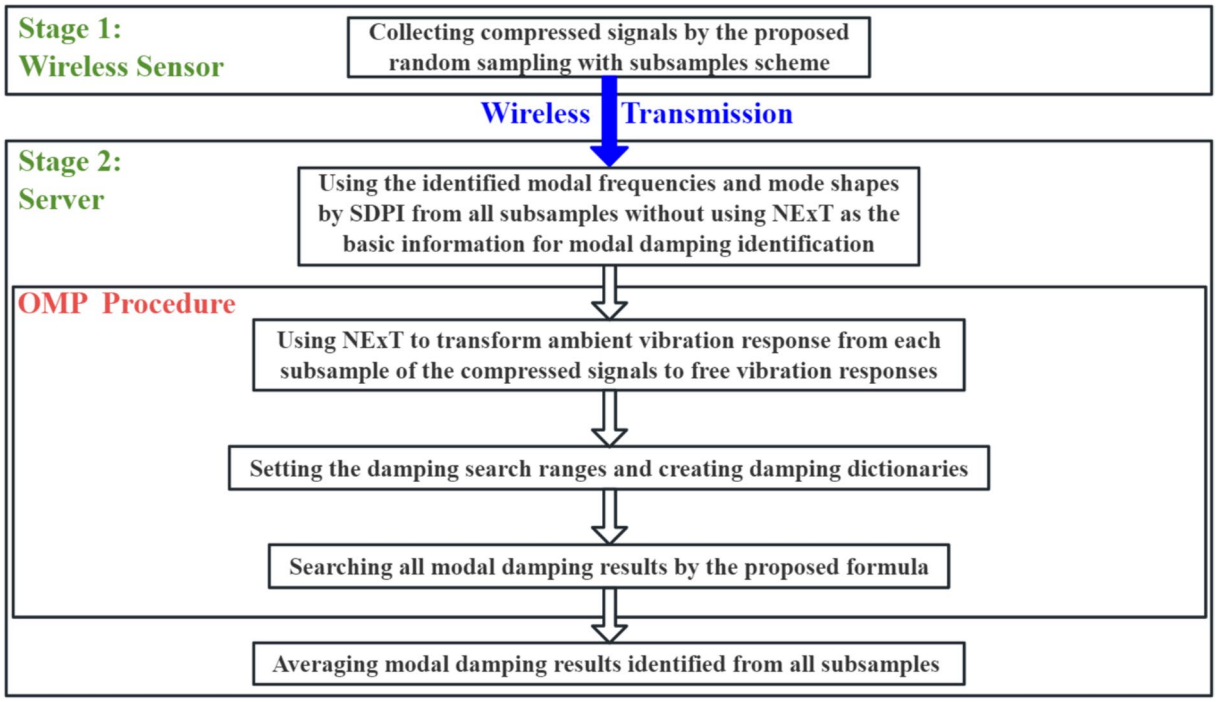

Fig. 2 Flowchart of the DISD method

as the basic information for modal damping identification. When the identified mode shapes are also considered as the basic information, the known information about the modes of interest rises. Therefore, the solutions of Eq. (5) can be more accurate based on the proposed identification order. Compared to the existing identification order, the proposed order can effectively enhance the performance of CS-based modal damping identification.

The existing formula of SDPI for modal damping identification [25] is:

$$\begin{aligned}&\text{Arg max}\left(\left\|\left[\mathbf{Y}\left(d'\boldsymbol{\Phi}\right)^{\mathrm{T}};\mathbf{Y}\left(d''\boldsymbol{\Phi}\right)^{\mathrm{T}}\right]\right\|_2\right)\text{s.t.}\\&\mathbf{d}'\in\mathbf{D}_{\xi=\{1,\ldots,q\}'},\mathbf{d}''\in\mathbf{D}''_{\xi=\{1,\ldots,q\}}\end{aligned}\tag{9}$$

Here, we propose a new formula to realize CS-based modal damping identification as below:

$$\begin{aligned}&\text{Arg max}\left(\left\|\left[\mathbf{R}\left(\boldsymbol{\psi}d'\boldsymbol{\Phi}\right)^{\mathrm{T}},\mathbf{R}\left(\boldsymbol{\psi}d''\boldsymbol{\Phi}\right)^{\mathrm{T}}\right]\right\|_{\mathrm{F}}\right)\text{ s.t.}\\&d'\in\mathbf{D}_{\xi=\{1,\ldots,q\}'},d''\in\mathbf{D}''_{\xi=\{1,\ldots,q\}}\end{aligned}\tag{10}$$

Compared to the existing formula of SDPI in Eq. (9), Eq. (10) adds the mode shapes as the known information and replaces the compressed measurements $\mathbf{Y}$ by the cross-correlation function $\mathbf{R}$. As a consequence, the inner product results between the atoms in dictionary $\mathbf{D}$ and the cross-correlation function $\mathbf{R}$ become a $N\times 2Q$ matrix rather than a vector for SDPI. As the number of elements of inner product results increases, more data is used to calculate the norm by OMP. Therefore, the proposed formula of DISD can achieve higher performance. For comparison, we replace the proposed formula Eq. (10) in DISD with the existing formula Eq. (9) used in SDPI to form another approach, namely Damping Identification by Sparse Decomposition with Existing Formula (DISDEF).

For each subsample, the modal damping results are estimated by solving Eq. (10). To avoid the influence of outliers, the identified value would be deleted if the dictionary boundary is reached during the searching process. Furthermore, the final modal damping results are the average values identified by all subsamples. The performance of the extracted modal damping results is evaluated by the similarity $\left(1-\frac{|\xi_j-\hat{\xi}_j|}{\xi_j}\times 100\%\right)$ between the identified result $\hat{\xi}_j$ and reference value ξ_j.

3 Numerical verification

DISD, DISDEF, and the traditional methods AFDD and SSI-COV are compared using numerical examples. For comparison, the free vibration responses of all subsamples

generated by using NExT are used as the inputs of all methods to identify modal damping results. Different fringe scenarios and environmental impact factors are considered in this section.

The numerical 4-DOF damped system is shown in Fig. 3, where external forces $f_1, \ldots, f_4$ are applied to mass $m_1, \ldots, m_4$, respectively, and the acceleration responses $\ddot{x}_1, \ldots, \ddot{x}_4$, are obtained from mass $m_1, \ldots, m_4$, respectively.

For this numerical example, $\mathbf{M}$ is an identity matrix. $\mathbf{K}$ is:

$$\mathbf{K} = \begin{bmatrix} k_1+k_2 & -k_2 & 0 & 0 \\ -k_2 & k_2+k_3 & -k_3 & 0 \\ 0 & -k_3 & k_3+k_4 & -k_4 \\ 0 & 0 & -k_4 & k_4+k_5 \end{bmatrix} = \begin{bmatrix} 20 & -10 & 0 & 0 \\ -10 & 22 & -12 & 0 \\ 0 & -12 & 20 & -8 \\ 0 & 0 & -8 & 16 \end{bmatrix} \times 100 \text{ N m}^{-1} \tag{11}$$

The proportional damping matrix is $\mathbf{C} = \beta\mathbf{K} + \gamma\mathbf{M}$, where γ is set to a fixed constant of 0.1, and β is set to 0.0005 and 0.001. For $\beta = 0.0005$, the modal frequencies are $\omega_{d,1} = 2.95$ Hz, $\omega_{d,2} = 5.87$ Hz, $\omega_{d,3} = 7.70$ Hz, $\omega_{d,4} = 9.75$ Hz. For $\beta = 0.001$, the modal frequencies are $\omega_{d,1} = 2.95$ Hz, $\omega_{d,2} = 5.86$ Hz, $\omega_{d,3} = 7.70$ Hz, $\omega_{d,4} = 9.75$ Hz.

Stationary force ($\mathbf{F}$) is the Gaussian noise (mean value is 0 and variance is 1), and non-stationary excitation is the stationary random excitation multiplied by an exponential function with a fixed decay rate ($\exp(-0.0001t)$). The $4 \times 100{,}000$ acceleration matrix $\ddot{\mathbf{X}}$ is created via superposing modal responses [31]. The sampling frequency is 30 Hz. The sampled time is 3333.3 s, $t = 0, 0.033, \ldots, 3333.3$ s. Figure 4 illustrates the frequency-domain responses of the original uncompressed responses at $\beta = 0.0005$.

The time lag parameter for both AFDD and SSI-COV is set to 1 for consistency. For SSI-COV, the range of model order is 2–30. The setting of time lag is related to $\omega_{d,1}$, and the impact of model order range on the damping identification results is insignificant. Detailed information on the parameter setting of AFDD and SSI-COV can be referred to [12]. For consistency, both DISD and DISDEF adopt the same compressed measurements by the proposed random sampling with subsamples scheme in each analysis. Following [24, 25], the compression ratio (CR) is M/L (M is the uncompressed response length and L is the incomplete response length). CRs of 3.33 and 5 are considered, and the

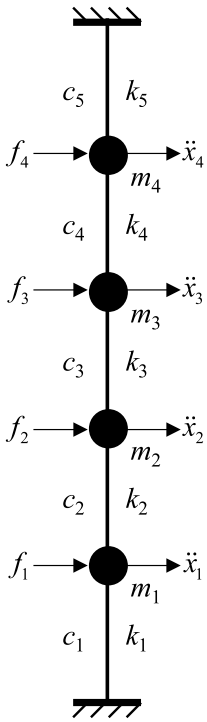

Fig. 3 The numerical 4-DOF damped system

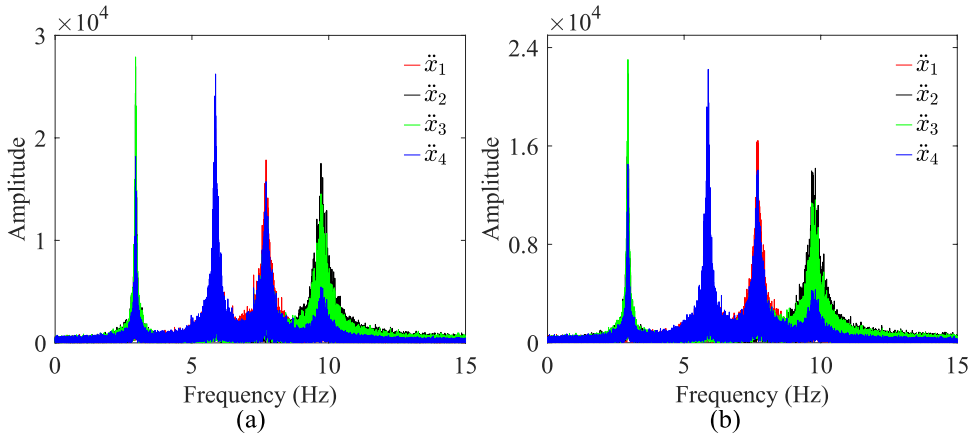

Fig. 4 The frequency spectrum of the original uncompressed acceleration under ambient vibration: **a** stationary excitation and **b** non-stationary excitation

incomplete response length is 30,000 and 20,000, respectively. The subsample length is set to 5000. The number of subsamples is 6 and 4 for CR = 3.33 and 5, respectively. For NExT, the reference channel is set to $\ddot{x}_1$, and the length of T is set to 2000. The cross-correlation function is a 4×2000 matrix. To keep consistency, the settings of NExT for both DISD and DISDEF are the same. The damping search ranges for both DISD and DISDEF are set to [0–10%] with a 0.005% interval. The number of atoms in dictionary **D** is 2001.

3.1 The explanations of parameter settings

Since the length of T in the NExT and the subsample length may have an influence on the accuracy of the results, the different settings of the two parameters are investigated.

First, the results using different lengths of T in the NExT are compared. The damping ratios identified by DISD and DISDEF are given in Table 1. As can be seen in Table 1, the accuracy of the identified mode 1 at $T = 1000$ and 3000 is lower than that at $T = 2000$ irrespective of method. The results of DISD are insensitive to different settings of the length of T. Overall, $T = 2000$ is appropriate for the numerical example.

Then, we study the results using different subsample lengths. Table 2 provides the damping ratios identified by DISD and DISDEF. We can find that the accuracy at subsample length = 3000, 4000, and 6000 is lower than that at subsample length = 5000 irrespective of method. The results of DISD and DISDEF are rather consistent with the reference at subsample length = 5000 and 6000. When the subsample length exceeds 5000, the results of DISD are insensitive to different settings of the subsample length. Therefore, subsample length = 5000 is suitable for the numerical example.

3.2 The stationary ambient vibration case

The accuracy of DISD is compared with that of DISDEF under different CRs and damping levels to demonstrate the performance of the proposed method. Here, we study the accuracy of different CS-based methods under a single environmental impact factor: ambient excitation. For consistency, we use identical compressed measurements **Y** irrespective of method. The damping ratios identified by DISD and DISDEF are shown in Table 3. It can be found that the damping ratios of the numerical system identified by both methods are close to true values irrespective of CR and damping level. Thus, the compressed measurements collected by the proposed random compression sampling scheme can successfully satisfy the requirement of NExT. The accuracy of both DISD and DISDEF is 98% at the lower damping level of $\beta = 0.0005$. The accuracy of DISD is mostly higher than that of DISDEF when the damping level of the numerical system increased to $\beta = 0.001$. The results of DISD are much better than that of the traditional methods AFDD and SSI-COV. The CS techniques need shorter measurement lengths, while AFDD and SSI-COV need longer measurement lengths to obtain accurate results [25]. Although DISD needs shorter subsample lengths, the length of the subsamples should be more than 5000, otherwise the error of the results of DISD may increase significantly. The results show that the proposed random compression scheme is more suitable for CS-based technique DISD than the traditional techniques AFDD and SSI-COV. The accuracy of the results of CS-based methods is much higher than that of the

Table 1 The modal damping ratios identified by DISD and DISDEF using different lengths of T at $\beta = 0.0005$ and CR = 5

Length of T	Mode	Damping ratio (%)			Accuracy (%)	
		References[a]	DISD	DISDEF	DISD	DISDEF
1000	1	0.733	0.776[b]	0.776	94.08	94.08
	2	1.057	0.976	0.993	92.35	93.89
	3	1.313	1.323	1.334	99.30	98.45
	4	1.614	1.573	1.574	97.44	97.52
2000	1	0.733	0.735	0.735	99.71	99.71
	2	1.057	0.991	1.008	93.77	95.31
	3	1.313	1.323	1.334	99.30	98.45
	4	1.614	1.573	1.574	97.44	97.52
3000	1	0.733	0.598	0.598	81.53	81.53
	2	1.057	0.993	1.008	93.89	95.31
	3	1.313	1.323	1.334	99.30	98.45
	4	1.614	1.574	1.575	97.52	97.60

[a]"Reference" represents the theoretical values of the original responses

[b]The value is the mean value of the results from all subsamples

Table 2 The modal damping ratios identified by DISD and DISDEF using different subsample lengths at $\beta = 0.001$ and subsample number = 4

Subsample length	Mode	Damping ratio (%)			Accuracy (%)	
		Reference	DISD	DISDEF	DISD	DISDEF
3000	1	1.196	1.018	1.028	85.10	85.94
	2	1.979	2.061	2.173	95.82	90.20
	3	2.523	1.658	1.690	65.69	66.97
	4	3.146	3.318	3.430	94.55	90.97
4000	1	1.196	1.153	1.160	96.46	97.02
	2	1.979	2.246	2.390	86.47	79.20
	3	2.523	2.260	2.345	89.56	92.93
	4	3.146	2.979	2.965	94.68	94.25
5000	1	1.196	1.219	1.228	98.07	97.34
	2	1.979	1.990	2.090	99.42	94.37
	3	2.523	2.530	2.569	99.74	98.20
	4	3.146	3.035	3.034	96.47	96.43
6000	1	1.196	1.255	1.259	95.04	94.72
	2	1.979	1.971	2.051	99.63	96.32
	3	2.523	2.618	2.688	96.27	93.50
	4	3.146	2.945	2.941	93.61	93.49

Table 3 The modal damping ratios identified by DISD and DISDEF under stationary ambient vibration

β	CR	Mode	Damping ratio (%)					Accuracy (%)			
			Reference	DISD	DISDEF	AFDD	SSI-COV	DISD	DISDEF	AFDD	SSI-COV
0.0005	3.33	1	0.733	0.708	0.709	0.502	0.492	96.65	96.76	67.16	67.16
		2	1.057	1.089	1.105	0.351	0.710	96.97	95.47	67.14	67.14
		3	1.313	1.296	1.312	0.514	0.851	98.67	99.87	64.77	64.77
		4	1.614	1.627	1.628	0.760	1.053	99.20	99.15	65.25	65.25
	5	1	0.733	0.735	0.735	0.493	0.447	99.71	99.71	61.03	61.03
		2	1.057	0.991	1.008	0.264	0.603	93.77	95.31	57.03	57.03
		3	1.313	1.323	1.334	0.508	0.724	99.30	98.45	55.14	55.14
		4	1.614	1.573	1.574	0.644	0.851	97.44	97.52	52.75	52.75
0.001	3.33	1	1.196	1.140	1.144	0.514	0.502	95.35	95.69	42.00	42.00
		2	1.979	1.942	2.021	0.683	1.421	98.14	97.86	71.80	71.80
		3	2.523	2.528	2.593	1.120	1.560	99.80	97.23	61.81	61.81
		4	3.146	3.138	3.132	1.631	2.015	99.76	99.55	64.06	64.06
	5	1	1.196	1.219	1.228	0.615	0.854	98.07	97.34	71.47	71.47
		2	1.979	1.990	2.090	0.777	1.300	99.42	94.37	65.70	65.70
		3	2.523	2.530	2.569	1.207	1.706	99.74	98.20	67.63	67.63
		4	3.146	3.035	3.034	1.630	2.399	96.47	96.43	76.26	76.26

traditional methods. DISD is slightly better than DISDEF under stationary ambient vibration.

We further investigate the impact of noise. Since AFDD and SSI-COV show worse accuracy, they are not compared. 20% and 30% Gaussian white noise is added to the complete responses. As noise is added, the number of environmental impact factors is two: noise and ambient excitation. Figure 5 illustrates the frequency-domain responses of the noisy responses. The estimated modal damping ratios at $\beta = 0.001$ and CR = 5 are shown in Table 4. According to Table 4, we find that DISD can identify all modal damping ratios accurately even at a high noise level of 30% under stationary ambient excitation. The accuracy of DISD is still higher than that of DISDEF. Compared to the single environmental impact factor cases, the proposed DISD under the two environmental impact factors realizes a higher performance. Overall, the anti-noise-interference performance of DISD is higher than DISDEF under stationary ambient excitation.

3.3 The non-stationary ambient vibration case

In this subsection, we further verify the effect of non-stationary ambient vibration on the modal damping ratios identified by different CS-based methods (DISD and DISDEF). Since the non-stationary factor is added, the number of environmental impact factors is two: nonstationarity and ambient excitation. As the excitation is polluted by the exponential function, the variation of excitation can reach roughly 30%. In such case, the excitation no longer follows the Gaussian distribution, therefore, the modal damping identification becomes rather challenging. The results for the case with $\beta = 0.0005$ are shown in Table 5. We discover that DISD can achieve accurate modal damping identification even for the case of the maximum decay of excitation up to 30%. Specifically, DISD is more accurate than DISDEF irrespective of CR for most cases. Compared to the results in Sect. 3.2, DISD can keep the advantage of accuracy when the non-stationary factor is added. Therefore, we draw the conclusion that DISD shows a higher performance than DISDEF under non-stationary ambient excitation.

Next, we compare the noise impact under non-stationary ambient excitation. The noise levels are 20% and 30%. As noise is introduced, the number of environmental impact factors is three: noise, nonstationarity, and ambient excitation. Figure 6 visualizes the frequency-domain responses of the

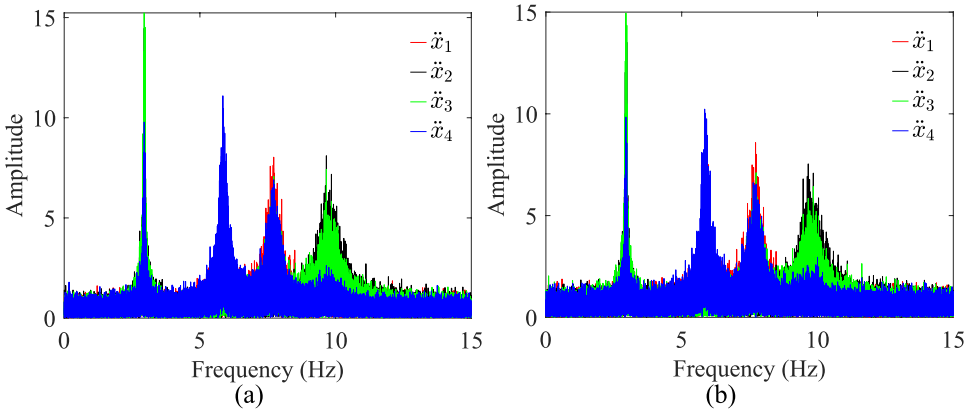

Fig. 5 The frequency spectrum of the responses with noise under stationary ambient vibration: **a** 20% noise and **b** 30% noise

Table 4 The modal damping ratios identified by DISD and DISDEF under stationary ambient vibration ($\beta = 0.001$ and CR = 5)

Noise percentage (%)	Mode	Damping ratio (%)			Accuracy (%)	
		Reference	DISD	DISDEF	DISD	DISDEF
20	1	1.196	1.195	1.203	99.95	99.43
	2	1.979	2.020	2.131	97.90	92.28
	3	2.523	2.530	2.616	99.74	96.32
	4	3.146	3.080	3.056	97.90	97.15
30	1	1.196	1.179	1.185	98.59	99.11
	2	1.979	2.151	2.246	91.27	86.47
	3	2.523	2.508	2.575	99.37	97.95
	4	3.146	3.129	3.109	99.45	98.82

Table 5 The modal damping ratio results of DISD and DISDEF under non-stationary ambient vibration ($\beta = 0.0005$)

CR	Mode	Damping ratio (%)			Accuracy (%)	
		Reference	DISD	DISDEF	DISD	DISDEF
3.33	1	0.733	0.686	0.688	93.58	93.81
	2	1.057	1.058	1.071	99.88	98.70
	3	1.313	1.323	1.333	99.24	98.48
	4	1.614	1.512	1.511	93.67	93.62
5	1	0.733	0.778	0.780	93.91	93.57
	2	1.057	1.073	1.098	98.54	96.18
	3	1.313	1.356	1.368	96.73	95.88
	4	1.614	1.614	1.616	100.00	99.85

noisy responses. For consistency, the same noisy measurements are adopted for DISD and DISDEF. The estimated modal damping ratios at $\beta = 0.0005$ and CR = 5 are shown in Table 6. From Table 6, we discover that DISD can identify all modal damping ratios accurately even at the high noise level of 30% under non-stationary ambient excitation. Still, DISD is more accurate than DISDEF irrespective of noise level. Even for the fringe scenario under three environmental impact factors, DISD can keep the advantage of accuracy. In summary, we concede that the anti-noise-interference performance of DISD is better than DISDEF under non-stationary ambient excitation.

4 Real monitoring data verification

In this section, we evaluate the performance of the proposed DISD using real monitoring data where multiple environmental impact factors exist simultaneously. The acceleration samples from an in-service long-span suspension bridge, the Tsing Ma bridge, under ambient vibration are used in this section. The schematic diagram of the bridge is shown in Fig. 7. The bridge has two decks, the upper and lower decks are used for expressway and railway, respectively. As the environmental conditions in the real world are extremely complex, the bridge was subjected to multiple environmental impact factors, such as ambient excitation, heavy noise,

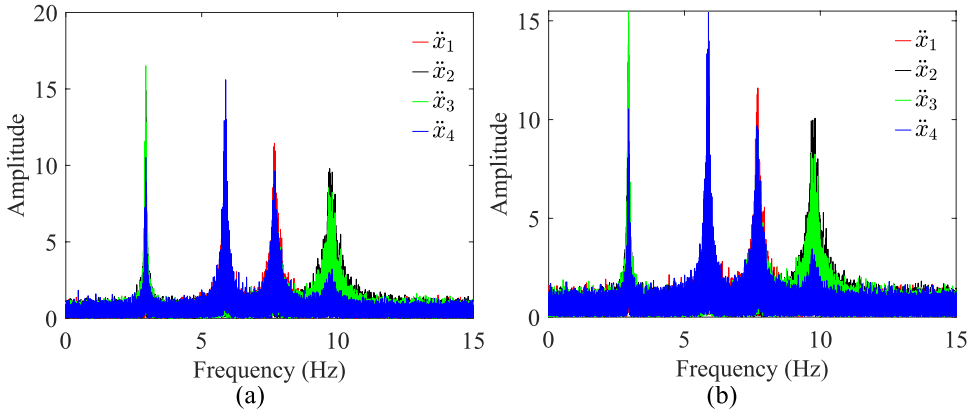

Fig. 6 The frequency spectrum of the responses with noise under non-stationary ambient vibration: **a** 20% noise and **b** 30% noise

Table 6 The modal damping ratios identified by DISD and DISDEF under non-stationary ambient vibration ($\beta = 0.0005$ and CR = 5)

Noise percentage (%)	Mode	Damping ratio (%)			Accuracy (%)	
		Reference	DISD	DISDEF	DISD	DISDEF
20	1	0.733	0.698	0.699	95.17	95.34
	2	1.057	1.124	1.149	93.69	91.33
	3	1.313	1.276	1.283	97.18	97.65
	4	1.614	1.620	1.621	99.61	99.54
30	1	0.733	0.825	0.835	87.43	86.07
	2	1.057	1.040	1.065	98.38	99.25
	3	1.313	1.341	1.364	97.88	96.16
	4	1.614	1.574	1.570	97.52	97.29

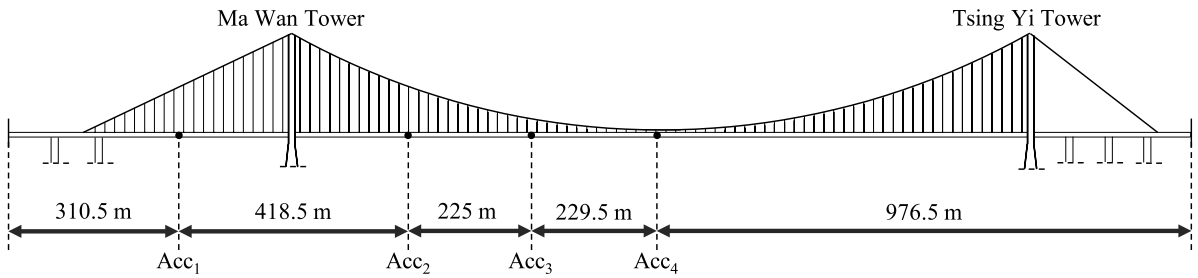

Fig. 7 Schematic diagram of Tsing Ma bridge

and nonstationarity [34–38]. Under such situation, modal identification becomes much more challenging.

A long-term SHM system, namely wind and structural health monitoring system, was installed on the Bridge in 1997. The system includes 276 sensors in seven types, which are used to measure wind speed, acceleration, temperature, strain, displacement, and liquid level. The original vertical acceleration samples are collected by four accelerometers (Acc_1, Acc_2, Acc_3, and Acc_4) installed on the deck of the bridge as shown in Fig. 7. It should be noted that only half of the bridge is equipped with accelerometers because the bridge is symmetric. The original sampled frequency is 51.2 Hz. To reduce high-frequency noise, the adopted datasets are down-sampled to 5.12 Hz. The response length is 50,000 for each analysis. The sampling length is enough for modal damping identification.

Figure 8 shows the time history and frequency-domain response of the uncompressed measurements. The modal frequency range of interest is [0–1 Hz]. The acceleration responses of the bridge are polluted by high-frequency noise. Therefore, we eliminate the signal components whose frequency exceeds 1 Hz through a lowpass filter. Figure 9 shows the time history and frequency-domain response of the filtered measurements. The filtered measurements are used for the uncompressed responses for modal damping identification.

The time lag of AFDD and SSI-COV is set to 50. For SSI-COV, the model order range is 2–60. For the CS-based methods, the considered CRs are 1.25, 1.67, 2.5, and 5 (the corresponding subsample numbers are 4, 3, 2, and 1, respectively). Each subsample length is set to 10,000. The reference channels of NExT are set to [Acc_1, Acc_2, Acc_3, Acc_4]. The length of T is set to 3000, therefore, the

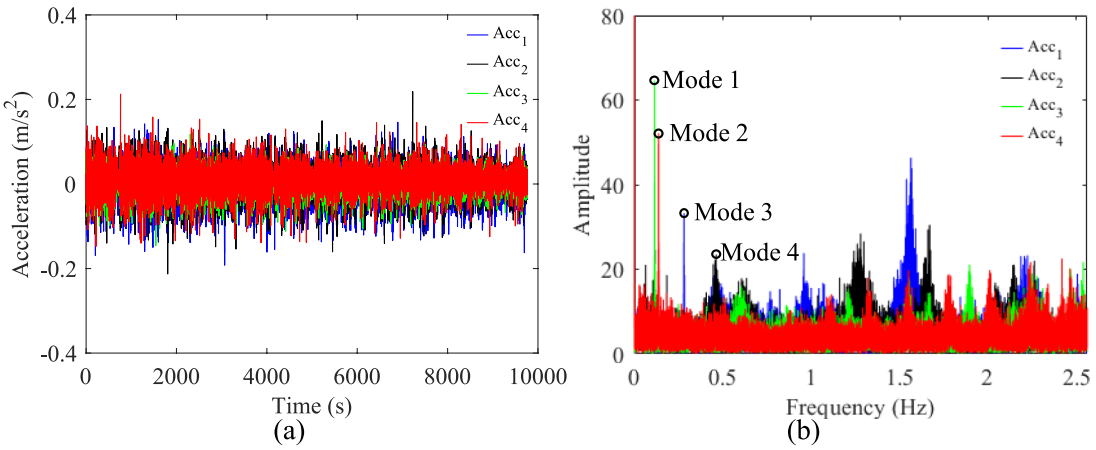

Fig. 8 The measurements of the bridge: **a** time history and **b** frequency spectrum

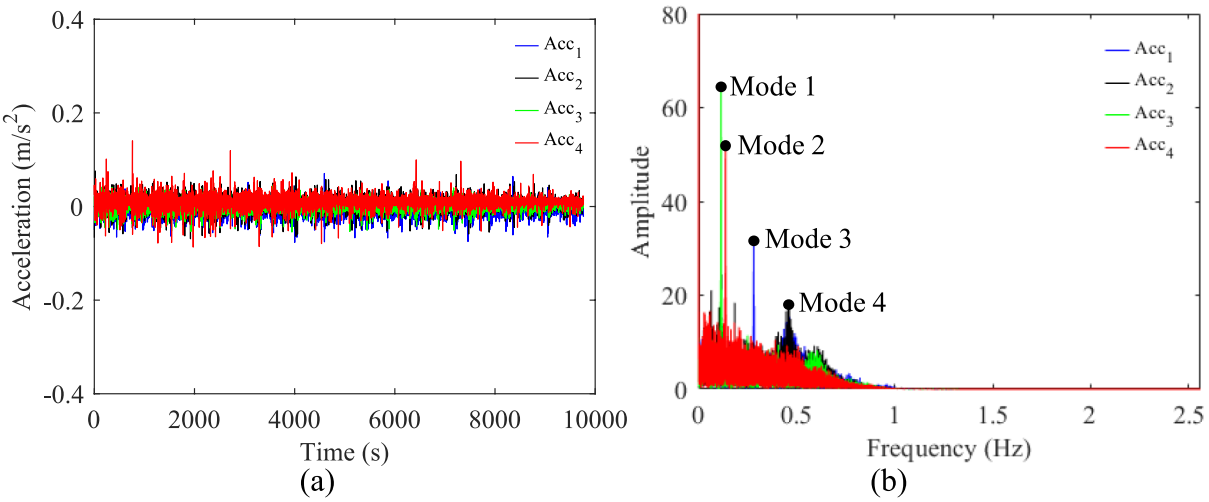

Fig. 9 The filtered measurements of the bridge: **a** time history and **b** frequency spectrum

cross-correlation function is a 16×3000 matrix. The settings of NExT for DISD and DISDEF are the same. The damping search ranges for both DISD and DISDEF are set to [0–10%] with a 0.005% interval. The number of atoms in dictionary **D** is 2001.

Modal damping ratios of the 4 dominated modes identified by AFDD and SSI-COV applied to the uncompressed measurements are studied. The identified modal frequencies of the four modes are 0.114 Hz, 0.137 Hz, 0.280 Hz, and 0.461 Hz (corresponding to the modes 1–4 in Figs. 8, 9). The frequencies of the modes 1–4 are close to those in Zhou et al. [35]. Note that there might be modes excited with modal frequencies higher than 1 Hz as shown in Fig. 8. However, these potential high-frequency modes are not convincing, and they contain a large level of noise. To reduce error, the mean value of the damping results of five original uncompressed measurements is used. The mode shapes are displayed in Fig. 10. The modal damping results are listed in Table 7. The identified damping results of the mode 1 of the two methods are close, while the damping results of the modes 2–4 of the two methods are rather different. Therefore, the mode 1 is considered for the following comparison between DISD and DISDEF. Note that SSI-COV may fail to capture some modes of interest, therefore, the results by AFDD are considered as the approximated reference.

Table 7 The modal damping ratios identified by AFDD and SSI-COV using five original uncompressed measurements

Mode	AFDD	SSI-COV
1	0.866	0.832
2	1.224	0.787
3	2.540	0.394
4	4.518	5.453

To explain the setting of parameters, we study the impact of different parameter settings of the length of T in the NExT and the subsample length on the accuracy of DISD and DISDEF. The results using different lengths of T in the NExT are compared. The modal damping ratios identified by DISD and DISDEF using different lengths of T are shown in Table 8, where the results of the approximated reference (copied from Table 7) use five original uncompressed measurements, while DISD and DISDEF use one compressed measurement (CR = 2.5). From Table 8, the accuracy of DISD and DISDEF at $T = 1000$, 2000, and 4000 is lower than that at $T = 3000$. In conclusion, $T = 3000$ is suitable for

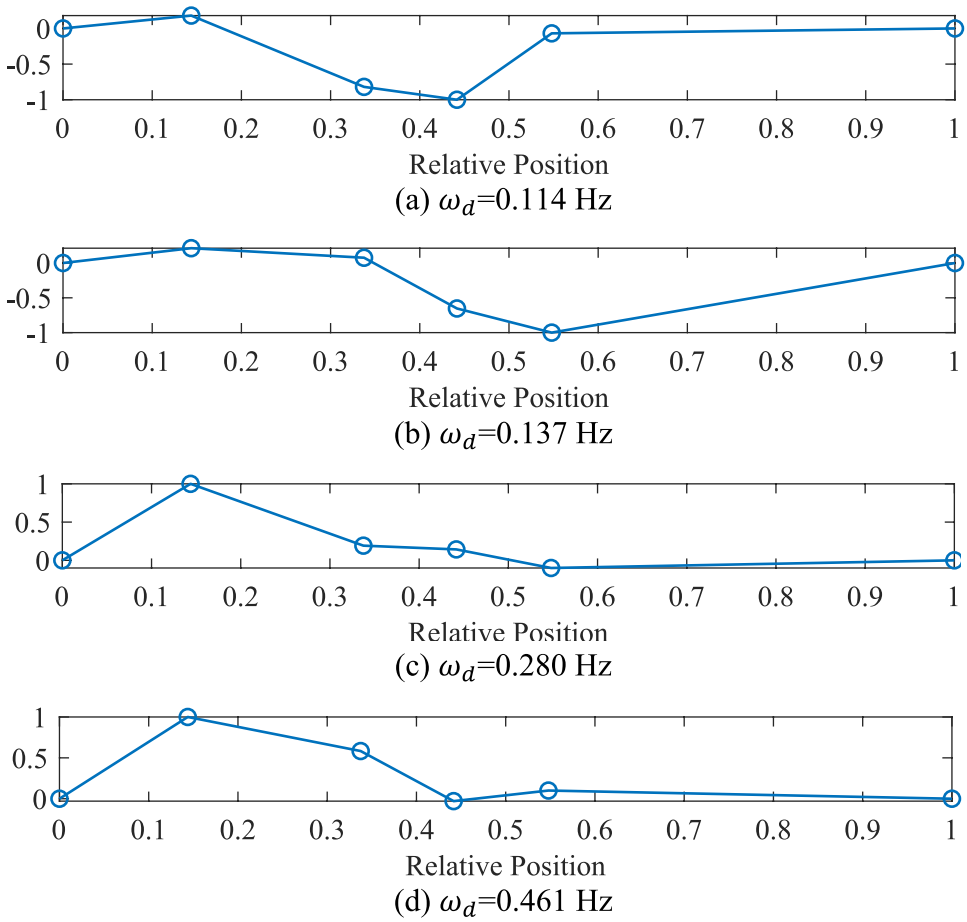

Fig. 10 The mode shapes identified by AFDD: **a** the mode 1, **b** the mode 2, **c** the mode 3, and **d** the mode 4

the damping identification of the bridge using DISD and DISDEF.

Next, we compare the results using different subsample lengths. The damping ratios identified by DISD and DISDEF use compressed measurements are listed in Table 9. We can find that the accuracy at subsample length = 8000, 9000, and 11,000 is lower than that at subsample length = 10,000 irrespective of method. The results of DISD and DISDEF are consistent with the approximated reference at subsample length = 10,000. Therefore, subsample length = 10,000 is appropriate for the damping identification of the bridge by DISD and DISDEF.

We also study the accuracy of different CS-based methods considering different environmental impact factors, such as traffic loads and temperatures. The performance of DISD and DISDEF at various hours is compared. The datasets in 0:00–3:00, 3:00–6:00, 6:00–9:00, 9:00–12:00, 12:00–15:00, 15:00–18:00, 18:00–21:00, and 21:00–24:00 are adopted for investigations. Table 10 provides the results at various time at CR = 2.5. Table 10 shows that DISD (around 95%) has higher accurate results than DISDEF (around 72%). The results of DISDEF are more robust than those of DISDEF since DISDEF may lose the mode of interest. In summary, DISD has higher performance than DISDEF using the responses of the bridge at various time.

Table 11 lists the estimated modal damping ratios at different CRs. DISD (91%) can obtain much more accurate modal damping results than DISDEF (56%) even for the compressed measurements. The accuracy of DISD is close at CR = 1.25, 1.67, and 2.5, while that of DISD is lower at CR = 5. The accuracy of DISDEF is more unstable as DISDEF may lose the mode of interest at CR = 5. The results of DISD and DISDEF at CR = 1.67 have the highest accuracy. Therefore, the recommended CR value is 1.67. In conclusion, DISD performs better than DISDEF using the real monitoring data of the bridge at different CRs.

Table 8 The modal damping ratios identified by DISD and DISDEF using different lengths of T at CR = 2.5

Length of $\boldsymbol{T}$	Mode	Damping ratio (%)			Accuracy (%)	
		Approximated reference[a]	DISD	DISDEF	DISD	DISDEF
1000	1	0.866	0.655	0.668	75.67	77.11
2000	1	0.866	0.693	0.703	80.00	81.15
3000	1	0.866	0.875	0.878	98.92	98.63
4000	1	0.866	0.778	0.785	89.82	90.68

[a]"Approximated reference" represents the modal damping results of AFDD calculated previously as listed in Table 7

Table 9 The modal damping ratios identified by DISD and DISDEF using different subsample lengths at subsample number = 2

Subsample length	Mode	Damping ratio (%)			Accuracy (%)	
		Approximated reference	DISD	DISDEF	DISD	DISDEF
8000	1	0.866	0.655	0.660	75.67	76.24
9000	1	0.866	0.795	0.790	91.84	91.26
10,000	1	0.866	0.875	0.878	98.92	98.63
11,000	1	0.866	0.943	1.068	91.12	76.68

Table 10 The modal damping ratios identified by DISD and DISDEF at various time at CR = 2.5

Mode 1	Damping ratio (%)							
	0:00–3:00	3:00–6:00	6:00–9:00	9:00–12:00	12:00–15:00	15:00–18:00	18:00–21:00	21:00–24:00
Approximated reference[a]	0.828	0.841	1.370	0.842	0.952	1.095	1.076	0.751
DISD	0.855	0.790	1.300	0.815	1.010	1.040	0.980	0.773
DISDEF	0.868	0.305	–	0.765	1.023	1.040	1.400	0.778
Accuracy of DISD	96.72	93.96	94.90	96.75	93.94	94.99	91.06	97.15
Accuracy of DISDEF	95.21	36.27	–	90.81	92.63	94.99	69.91	96.49

[a]"Approximated reference" represents the modal damping results of AFDD using one original uncompressed measurement

Table 11 The modal damping ratios identified by DISD and DISDEF at different CRs

CR	Mode	Damping ratio (%)			Accuracy (%)	
		Approximated reference	DISD	DISDEF	DISD	DISDEF
1.25	1	0.778	0.833	0.885	92.97	86.22
1.67	1	0.778	0.770	0.832	98.99	93.08
2.5	1	0.778	0.845	0.345	91.37	44.35
5	1	0.778	0.625	–	80.35	–

5 Conclusions

This study proposes a modal damping identification method named DISD with a new random compression sampling scheme and a new identification formula. To verify the effectiveness of the proposed method, cases of a simple numerical system and the Tsing Ma bridge are studied. We also compare the performance of the proposed formula with that of DISDEF, AFDD, and SSI-COV under different fringe scenarios and environmental impact factors. Based on the study, two conclusions can be drawn:

- The proposed random compression sampling scheme can be adopted for CS-based OMA methods to satisfy the requirement of NExT. Thus, modal damping can be easily identified via CS techniques under ambient vibration. The scheme is more suitable for CS-based methods, e.g., DISD, than the conventional techniques, such as AFDD and SSI-COV.
- DISD displays a high performance in complex cases, e.g., ambient excitation, heavy noise, and nonstationarity. The method can achieve the same accuracy under more environmental impact factors as under less environmental impact factors. Compared to DISDEF, DISD realizes a higher accuracy (up to 35% improvement). Therefore, we concede that DISD has the potential to be an efficient online SHM tool for engineering structures.

The following directions for future research can be concentrated on: (i) the correlations between damping results and environmental factors; (ii) the robustness of the proposed framework against nonstationarity.

Acknowledgements This research has been supported by the start-up fund for research assistant professors under the strategic hiring scheme of the Hong Kong Polytechnic University (Grant No. P0046770). The authors also appreciate the funding support by the Innovation and Technology Commission of Hong Kong SAR Government to the Hong Kong Branch of Chinese National Rail Transit Electrification and Automation Engineering Technology Research Centre (Grant No. K-BBY1). The authors also wish to thank the Hong Kong SAR Government Highways Department for providing the long-term structural health monitoring data of the Tsing Ma Bridge.

Author contributions Jian Zhou: conceptualization, methodology, investigation, software, formal analysis, data curation, visualization, writing—original draft, writing—review and editing. Hong-Wei Li: methodology, validation, supervision, writing—review and editing. You-Wu Wang: validation, supervision, writing—review and editing. Yi-Qing Ni: supervision, resources, funding acquisition, writing—review and editing.

Funding Open access funding provided by The Hong Kong Polytechnic University.

Data availability Data will be made available on request.

Declarations

Conflict of interest The authors declare that they have no known competing financial interests or personal relationships that could have appeared to influence the work reported in this paper.

References

1. Ko JM, Ni YQ (2005) Technology developments in structural health monitoring of large-scale bridges. Eng Struct 27(12):1715–1725
2. Wang YW, Ni YQ, Wang SM (2022) Structural health monitoring of railway bridges using innovative sensing technologies and machine learning algorithms: a concise review. Intell Transp Infrastruct. https://doi.org/10.1093/iti/liac009
3. Sivasuriyan A, Vijayan DS, Munusami R, Devarajan P (2021) Health assessment of dams under various environmental conditions using structural health monitoring techniques: a state-of-art review. Environ Sci Pollut Res 29:86180–86191

4. Li Q, He Y, Zhou K, Han X, He Y, Shu Z (2018) Structural health monitoring for a 600 m high skyscraper. Struct Design Tall Spec Build 27(12):e1490
5. Fan G, Li J, Hao H (2019) Improved automated operational modal identification of structures based on clustering. Struct Control Health Monit 26(12):e2450
6. Hou R, Xia Y (2021) Review on the new development of vibration-based damage identification for civil engineering structures: 2010–2019. J Sound Vib 491:115741
7. Li B, Au SK (2019) An expectation-maximization algorithm for Bayesian operational modal analysis with multiple (possibly close) modes. Mech Syst Signal Process 132:490–511
8. Yuan K, Zhu WD (2023) Identification of modal parameters of a model turbine blade with a curved surface under random excitation with a three-dimensional continuously scanning laser Doppler vibrometer system. Measurement 214:112759
9. Han Y, Wu G, Feng D (2023) Structural modal identification using a portable laser-and-camera measurement system. Measurement 214:112768
10. Klis R, Chatzi E (2017) Vibration monitoring via spectro-temporal compressive sensing for wireless sensor networks. Struct Infrastruct Eng 13:195–209
11. Abdulkarem M, Samsudin K, Rokhani FZ, A Rasid MF (2020) Wireless sensor network for structural health monitoring: a contemporary review of technologies, challenges, and future direction. Struct Health Monit 19(3):693–735
12. Cheynet E, Jakobsen JB, Snæbjörnsson J (2017) Damping estimation of large wind-sensitive structures. Procedia Eng 199:2047–2053
13. Donoho DL (2006) Compressed sensing. IEEE Trans Inf Theory 52(4):1289–1306
14. Candès EJ, Romberg JK, Tao T (2006) Robust uncertainty principles: exact signal reconstruction from highly incomplete frequency information. IEEE Trans Inf Theory 52(2):489–509
15. Wang Y, Hao H (2010) An introduction to compressive sensing and its potential applications in structural engineering. In: The 11th international symposium on structural engineering, pp 1089–1094
16. Wang Y, Hao H (2015) Damage identification scheme based on compressive sensing. J Comput Civ Eng 29(2):04014037
17. Wan HP, Dong GS, Luo Y, Ni YQ (2022) An improved complex multi-task Bayesian compressive sensing approach for compression and reconstruction of SHM data. Mech Syst Signal Process 167:108531
18. Gkoktsi K, Giaralis A (2017) Assessment of sub-Nyquist deterministic and random data sampling techniques for operational modal analysis. Struct Health Monit 16(5):630–646
19. Gkoktsi K, Giaralis A, Klis RP, Dertimanis V, Chatzi E (2017) Vibration-based structural performance assessment via output only sub-Nyquist/compressive wireless sensor data. In: Proceedings of the 2017 conference on smart monitoring, assessment and rehabilitation of civil structures
20. Li S, Yang D, Tang G, Wakin MB (2018) Atomic norm minimization for modal analysis from random and compressed samples. IEEE Trans Signal Process 66(7):1817–1831
21. Yang Y, Nagarajaiah S (2019) Output-only modal identification by compressed sensing: non-uniform low-rate random sampling. Mech Syst Signal Process 56:15–34
22. Park JY, Wakin MB, Gilbert AC (2014) Modal analysis with compressive measurements. IEEE Trans Signal Process 62(7):1655–1670
23. Park JY, Wakin MB, Gilbert AC (2015) Sampling considerations for modal analysis with damping. In: Sensors and smart structures technologies for civil, mechanical, and aerospace systems, pp 283–293
24. Kang J, Duan Z (2020) Modal parameter identification with compressed samples by sparse decomposition using the free vibration function as dictionary. Smart Struct Syst Int J 25(2):123–133
25. Zhou J, Bence K, Wang Y (2023) Operational modal analysis with compressed measurements based on prior information. Measurement 211:112644
26. Al-Hababi T, Cao M, Saleh B, Alkayem NF, Xu H (2020) A critical review of nonlinear damping identification in structural dynamics: methods, applications, and challenges. Sensors 20(24):7303
27. Ay AM, Khoo S, Wang Y (2019) Probability distribution of decay rate: a statistical time-domain damping parameter for structural damage identification. Struct Health Monit 18(1):66–86
28. Xie F, Aly AM (2020) Structural control and vibration issues in wind turbines: a review. Eng Struct 210:110087
29. Tomac I, Slavič J (2022) Damping identification based on a high-speed camera. Mech Syst Signal Process 166:108485
30. Van Vondelen AAW, Navalkar ST, Iliopoulos A, Van Der Hoek DC, Van Wingerden JW (2022) Damping identification of offshore wind turbines using operational modal analysis: a review. Wind Energy Sci Discuss 7(1):161–184
31. James GH, Carne TG, Lauffer JP (1993) The natural excitation technique (NExT) for modal parameter extraction from operating wind turbines. Sandia National Labs, Albuquerque
32. Magalhaes F, Cunha A, Caetano E (2009) Online automatic identification of the modal parameters of a long span arch bridge. Mech Syst Signal Process 23(2):316–329
33. Tropp JA, Gilbert AC (2007) Signal recovery from random measurements via orthogonal matching pursuit. IEEE Trans Inf Theory 53(12):4655–4666
34. Lu F, Lin JH, Kennedy D, Williams FW (2009) An algorithm to study non-stationary random vibrations of vehicle–bridge systems. Comput Struct 87(3–4):177–185
35. Zhou XT, Ni YQ, Zhang FL (2014) Damage localization of cable-supported bridges using modal frequency data and probabilistic neural network. Math Probl Eng. https://doi.org/10.1155/2014/837963
36. Cheynet E, Jakobsen JB, Snæbjörnsson J (2016) Buffeting response of a suspension bridge in complex terrain. Eng Struct 128:474–487
37. He Y, Yang JP, Li YF (2022) A three-stage automated modal identification framework for bridge parameters based on frequency uncertainty and density clustering. Eng Struct 255:113891
38. Mao J, Su X, Wang H, Li J (2023) Automated Bayesian operational modal analysis of the long-span bridge using machine-learning algorithms. Eng Struct 289:116336